Polymers & biopolymers



Bacterial cellulose integrated irregularly shaped microcapsules enhance self-healing efficiency and mechanical properties of green soy protein resins

Shanshan Shi¹ and Anil N. Netravali^{1,*}

Received: 17 November 2020 Accepted: 30 March 2021 Published online: 13 April 2021

© The Author(s), under exclusive licence to Springer Science+Business Media, LLC, part of Springer Nature 2021

ABSTRACT

Soy protein isolate (SPI)-based self-healing thermoset resins were prepared using either poly(DL-lactide-co-glycolide) porous microspheres (MSs) and spherical microcapsules (MCs) or elongated MCs containing a combination of ground bacterial cellulose (GBC) and SPI as the healing agent. Spray emulsification, combined with solvent evaporation technique, was used to prepare MCs and MSs. The technique resulted in two MC morphologies: one primarily consisting of a mixture of porous MSs and spherical MCs and the other consisting of elongated MCs with aspect ratios as high as 50, depending on the surfactant and GBC amount used. While porous MSs made the resin stronger, they did not contribute to self-healing since they could not retain the healant. Part of the GBC, added during MC preparation, got successfully encapsulated into MCs to form strong GBC/SPI composite healtant. Most of the remaining GBC stayed on MC surfaces and was seen to enhance the MC/resin interfacial adhesion which, in turn, contributed to increased self-healing efficiency. Overall results indicated that resins with 20 wt% elongated MCs exhibited self-healing efficiencies of about 45% in strength and 59% in toughness. The results suggest that the integration of GBC in the healant could also work in other resin systems to enhance their self-healing efficiencies.

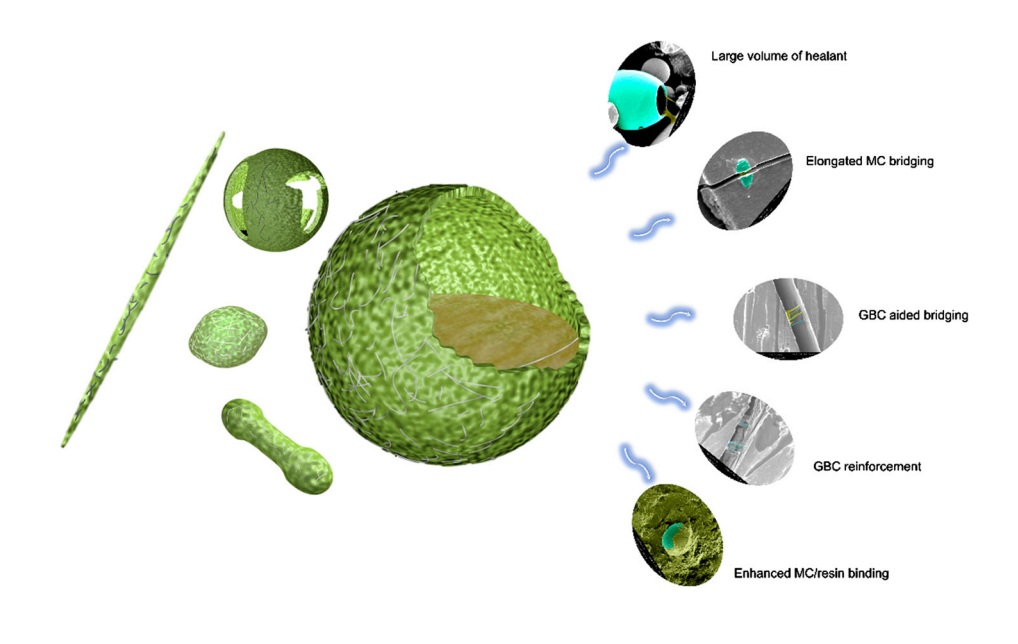
Handling Editor: Stephen Eichhorn.

Address correspondence to E-mail: ann2@cornell.edu



¹ Department of Fiber Science & Apparel Design, Cornell University, Ithaca, NY 14853, USA

GRAPHICAL ABSTRACT



Introduction

Plastics have become ubiquitous part of our daily life because of the advantages they offer over the weaknesses of metals, wood and ceramics which were predominantly used before polymers came into existence. While petroleum-derived conventional polymers have many desirable properties and are used in countless applications, there are two critical issues with their current use that have become obvious in recent years. The first issue is the sustainability of the petroleum supply itself. It has been estimated that world's petroleum reserves will not last for more than 5-6 decades at the current rate of consumption [1]. The second issue is the end of life disposal of plastics. Plastics do not degrade easily and linger for several centuries, contributing to land, water and air pollution [2].

To address the problems caused by conventional plastics, three different ways have been universally accepted, besides reducing their use. The first is to recycle the materials as many times as possible, the second is to use sustainable raw materials and the third is to prolong their service life using novel approaches. At present, significant amounts of

plastics and composites end up in landfills. Using biodegradable and yearly renewable resources such as plants to develop materials with properties similar to conventional plastics can have great advantages, and many efforts are being made in this direction. At the end of their life, they can be composted rather than ending up in landfills.

Plant-based resources are fully sustainable and enjoy many advantages such as plentiful availability, renewability and biodegradability. Soybean products in the form of defatted soy flour (SF), soy protein concentrate (SPC) or soy protein isolate (SPI) have been used as 'green' substitutes to replace conventional, petroleum-based polymers, resins and adhesives [3, 4]. Soy protein contains a number of amino acids with reactive groups such as carboxyl, hydroxyl and amine [5]. These reactive groups provide the opportunities for cross-linking which can significantly improve the mechanical properties of soy protein-based resins as well as composites [6].

Besides utilizing green raw materials and repeated recycling, prolonging the service life of materials is another effective solution to reduce our dependence on petroleum and has been successfully tried for polymers and composites [7–11]. All materials are



subjected to cumulative damages during their use because of the stresses endured. However, materials with self-healing characteristics have the ability to recover autonomously from such damages, fully or partially, and thus extend their useful life as well as safety during use. Two broad classes of self-healing systems: intrinsic and extrinsic healing, have been used in the past [12]. Intrinsic healing system requires polymers with a certain degree of molecular mobility which may be difficult to obtain in highly crosslinked thermoset resins, and as a result, extrinsic healing systems have been more commonly used [13, 14]. Extrinsic self-healing systems can be further divided into three distinct categories: microcapsule (MC)-based, microvascular and phase separation healing systems [15]. Among these, the MC-based self-healing system has been the most popular one because of the fabrication ease. MC-based self-healing systems have been used in a wide variety of materials such as concrete, metals, conventional polymers as well as natural polymers [16–18].

The MC-based self-healing system includes MCs that contain single healing agents such as resins or cross-linkers. However, dual-MC healing systems which include MCs that contain resin and cross-linkers, separately, have been found to be useful as well [18]. The most successful technique to prepare MCs has been the solvent evaporation method [19]. Various types of emulsion systems including the oil-in-water (O/W), water-in-oil (W/O) and complex emulsions have been used in the past to prepare MCs [20–23]. The water-in-oil-in-water (W/O/W) emulsion system has been one of the most successful methods of MC preparation [19]. Kim and Netravali successfully prepared spherical MCs using a green W/O/W system where a W/O emulsion containing SPI in water and poly(D, L-lactic-co-glycolic acid) (PLGA) dissolved in ethyl acetate was dispersed in polyvinyl alcohol (PVA) water solution [9]. Kim and Netravali also investigated the effects of various parameters including homogenization rate and concentration of PVA on the morphologies and sizes of MCs [24].

Bacterial cellulose (BC) nanofibers have high molecular orientation and crystallinity and have been used in numerous applications [25–27]. For example, BC and finely chopped (ground) BC (GBC) have been used in many diverse applications that include reinforcement, fat substitutes, medical devices and emulsion stabilizers [25, 26]. Kalashnikova et al. prepared Pickering emulsions using GBC as the

stabilizer and found that GBC remains on the surfaces of nanoparticles, which, in turn, helps with their dispersion [27].

Self-healing of conventional resins and composites has shown many advantages it can bring [15]. Self-healing green resins or composites being a newly developing area, very few studies have been published [22, 24, 28]. However, these studies have also shown that there is a need to improve MC/resin adhesion to increase the self-healing efficiency. A recently published review has also shown new possibilities in self-healing green composites [29].

In the present research, SPI-based self-healing resins were prepared and evaluated. Novel spray emulsification in combination with solvent evaporation technique was used to obtain much desired elongated MCs with aspect ratios as high as 50. In addition, GBC was incorporated during MC preparation. The technique also created GBC-coated spherical MCs that contained GBC and SPI as well as microspheres with holey shell geometry (MSs). Due to its exceptional tensile properties, GBC was expected to act as a reinforcing agent for the SPI, making it a composite healant that would be much stronger than SPI alone. Part of the GBC also covered MC surface creating textured topography. The benefit of MCs with GBC-coated textured or rough surface was to obtain better bonding with the resin and improve the self-healing efficiency by forming stronger healant bridges between the fracture surfaces. As the results have shown, MCs coated with GBC do adhere to the resin better. Part of the GBC present on the MC surfaces got incorporated in the resin and enhanced its tensile strength and fracture toughness.

Elongated MCs, with their higher aspect ratios, increased the probability of them being in the path of the microcracks. This higher probability helped to increase the self-healing efficiency of the resin. Though microspheres (MSs) with holey shell architecture could not contain any healant, they were found to enhance the resin mechanical properties.

Experimental

Materials

SPI (ProFam 974) was obtained as donation from Archer Daniels Midland Company. Poly(DL-lactide-co-glycolide) (50:50, PLGA), ester-terminated copolymer, with two different inherent viscosities of



1.15 dL/g and 1.20 dL/g in hexafluoroisopropanol (HFIP), were purchased from DURECT Corp., Birmingham, AL. Both performed identically and, hence, were used based on the availability of the polymer. Poly(vinyl alcohol) (PVA, average Mw 31,000–50,000, 98-99% hydrolyzed), sodium hydroxide pellets (NaOH, 97.0%), glutaraldehyde (GA, 25 wt% in $(\geq 99.8\%)$ water), ethvl acetate and polyvinylpyrrolidone (PVP) were purchased from Sigma-Aldrich (St. Louis, MO). Acetobacter (A. Xylinum), ATCC 23,769, bacterium was purchased from the American Type Culture Collection (ATCC, Manassas, VA) as the model strain. D-mannitol, yeast extract, tryptone and agar were acquired from Acros Organics (Thermo Fisher Scientific, Morris, NJ). Rhodamine B (dye) powder, Bradford reagent (0.1%), Coomassie blue R-250 (in a solution composed of 45% methanol, 10% acetic acid and deionized (DI) water at the ratio of 5:4:1) and sodium dodecyl sulfate (SDS) were bought from Sigma-Aldrich Chemical Co., Allentown, PA.

Preparation of BC pellicles

The freeze-dried *A. xylinum* obtained from ATCC was activated and cultivated in mannitol medium to obtain BC pellicles according to ATCC protocol. Further the BC pellicles were freeze-dried and ground to fine powder (GBC) to blend with the SPI healant. The detailed process of pellicle formation and grinding process to obtain GBC can be found in supplementary material.

Preparation of MCs and MSs

Spray emulsification combined with solvent evaporation technique was used to obtain MCs. Two types of MC morphologies, holey MSs and elongated MCs, were prepared using two sets of parameters. In the first set termed ST-I, a mixture of holey MSs and MCs was obtained. The holey MSs could not retain the healant because of their holey characteristics. The MCs were confirmed to contain the healant. In the second set termed ST-II, elongated MCs, with aspect ratios as high as 50, were formed. These MCs not only encapsulated both SPI and GBC inside them but were also covered with GBC. Both ST-I and ST-II specimens were prepared using spray emulsification in combination with solvent evaporation technique. Full

details of both ST-I and ST-II processes are provided in supplementary material.

Preparation of the self-healing green resins

SPI powder (10 gm) was added to 100 mL of DI water after which 8 mL of NaOH solution was added to achieve a pH of 14 to denature the SPI. This solution was stirred at 300 rpm for 15 min at 80 °C. Predetermined amounts of MCs based on different loadings (10, 20, 30 wt% of SPI powder) were mixed in the solution, separately, and stirred for 10 min. Crosslinker, GA (20 wt% of SPI powder), was then added to the mixture and stirring was continued for another 10 min. The resin was poured onto a flat Teflon®-coated sheet and allowed to partially cure/dry overnight in an air-circulating oven at 75 °C. The partially cured/dried resin sheets were hot-pressed at 80 °C under a small pressure of 7 MPa for 10 min to obtain 1-mm-thick cured resin sheets.

Self-healing test specimens were prepared from the resin sheets by cutting them into rectangular pieces with dimensions of $32 \text{ mm} \times 30 \text{ mm} \times 1 \text{ mm}$. They were then laser cut to the geometry shown in Fig. 1a, based on ASTM E647-08 [30]. In addition, a 40-deg arc was laser cut just below the crack tip at a distance of 10 mm. (The distance is measured from the tip of the pre-crack to the curvature.) The arc was specifically cut to capture and arrest the cracks after propagating for 10 mm, during the self-healing efficiency test. All specimens were kept in a desiccator for 3 days prior to performing self-healing efficiency tests.

Characterization for MCs/MSs

Scanning electron microscope (SEM) analysis

SEM, Leo 1550 SEM and Zeiss Gemini 500 FESEM were used to characterize the sizes, shapes and surface topographies of MCs/MSs. MC/MS suspensions, 0.5% (w/v), were prepared using DI water for SEM imaging. A drop of the suspension was placed on the conductive carbon tape glued to the SEM metal stub, and the water was allowed to evaporate. The stubs with specimens were coated with gold prior to SEM imaging.



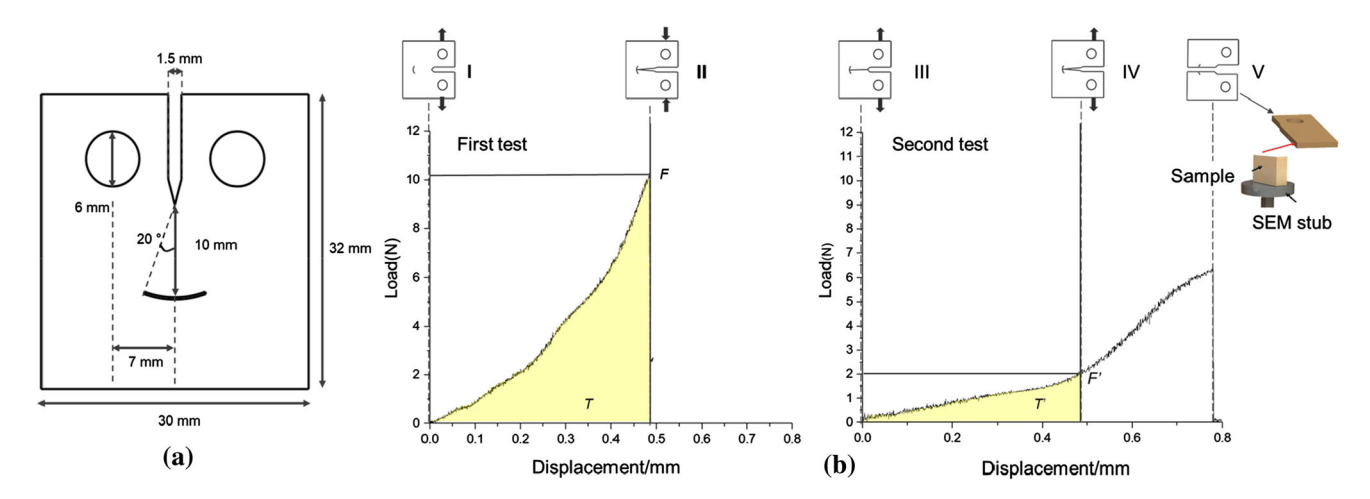


Figure 1 a Self-healing test specimen geometry; b load vs displacement plots during typical self-healing tests. I to V are the stages of the self-healing test.

Evaluation of protein loading in MCs/MSs

To release the protein contained inside the MCs/ MSs, 100 mg of MCs/MSs was subjected to milling. The milled powder was added to 10 mL of 10 mM NaOH containing 5% (w/v) SDS. The suspension was stirred for 2 h until it was clear and then was subjected to centrifugation at 5000 rpm for 10 min to get rid of the insoluble residues. An array of standard SPI solutions were prepared to set up a reference curve. The pH values of both sample solutions and standard SPI solutions were adjusted to 2 using a 0.5 mM HCl solution after which a desired amount of the Bradford agent was added to all samples until a blue color was observed. The protein loading was determined using the principle reported by Hora et al. which uses the maximum absorption at 595 nm on a UV/Vis spectrophotometer (PerkinElmer Lambda 35, Waltham, MA) [31].

Confocal laser scanning microscope (CLSM) analysis

The CLSM analysis was carried out on MCs, using Zeiss LSM 710 microscope equipped with 25 mW Argon and HeNe lasers, to confirm that they contained the healing agent (SPI slurry). For this, the SPI slurry was stained using Rhodamine B-water solution prior to encapsulating it in PLGA [22]. MCs were prepared using the same process described earlier in Sect. 3.2.2. These MCs were characterized using CLSM with a 63X oil immersion lens and associated filter for 514-nm wavelength excitation. Images were taken in both fluorescent and transmission modes.

Characterization of ground bacterial cellulose (GBC)

GBC nanofibers were characterized using SEM for their morphologies after each processing step, e.g., control (freeze-drying), after grinding and after grinding + ball milling.

Characterization of self-healing green resins

SEM analysis

Fracture surfaces obtained after completing the self-healing tests (stage V shown in Fig. 1b) of all resin specimens were characterized using SEM. Fractured specimens were mounted on double-sided conductive carbon tapes glued to the metal stub (as shown in stage V in Fig. 1b) with fracture surface on the top. Before taking the images, resin specimens were kept in a desiccator for 3 days at RT to remove the absorbed moisture.

Characterization of self-healing efficiency

The self-healing test was performed in two steps. The first step involved creating a 10 mm crack in the specimen by pulling the upper and lower parts using an Instron universal tester (Instron, Model 5566, Canton, MA) as shown in stage I in Fig. 1b. This initial 10 mm crack was designed to stop at the mouth-shaped arc, shown as stage II in Fig. 1b. Once the crack length of 10 mm was reached, the Instron was programmed to return the grips back to their starting point. The specimen was then removed from



the Instron. All tested specimens were kept in a sealed container for 24 h prior to performing the second step. In the second step, the specimens (after 24 h of healing, Fig. 1b, stage III) were placed individually in the Instron grips, which was programmed to pull (stage IV) and break the specimens into two pieces (stage V). Crosshead speed during both steps was maintained at 0.3 mm/min, as per ASTM E647-08 [30]. During the self-healing tests, the resin specimens were observed to undergo slight deformation which primarily included bending and stretching, both of which absorb some energy. The virgin resin was also observed to show a minor self-healing capability, perhaps due to the absorbed moisture.

The self-healing efficiencies were calculated in terms of strength (load at break) as well as toughness (areas under the curve in load vs displacement curve). Self-healing efficiency was defined as the ratio of the strength (or fracture toughness) of the healed resin to the virgin resin as shown in Eqs. (1) and (2) [32]. Self-healing efficiency in terms of strength (η_F) and toughness (η_T) was calculated using Eqs. 1 and 2, respectively, where F and F' (in Fig. 1b) correspond to the strength (resin failure load) values obtained in the first and the second tests, respectively, at the same displacement, and T and T' correspond to the toughness (yellow areas in Fig. 1b) in the first and second tests at the same displacement.

$$\eta_F = \frac{F' - F}{F} \times 100 \tag{1}$$

$$\eta_T = \frac{T' - T}{T} \times 100 \tag{2}$$

Tensile tests

Resin sheets containing MCs, MSs as well as control resin were shear cut to strips of $50 \text{ mm} \times 10 \text{ mm} \times 10$

Results and discussion

Morphologies and topographies of MCs and MSs

Figure 2 shows typical SEM images of ST-I MCs and holey MSs produced by the spray technique. MC and MS diameters and shell thicknesses were determined by randomly selecting intact and broken MCs within the SEM images taken, respectively, using ImageJ software. Some ST-I MSs shown in Fig. 2 exhibit a constellation of pores on the surfaces of spherical shells. These MSs have diameters that exceed 3 μ m. Smaller MCs that remained intact showed no holes. Obviously, MSs with holes cannot contain any SPI slurry (healant). This is the major reason why ST-I MCs/MSs exhibited the lowest protein loading (discussed later), and as a result, they were inefficient in providing any self-healing.

The shell thickness of these holey MSs was about 250 nm, and the pore diameters on the surfaces ranged from 1 μ m to about 2.5 μ m. This type of holey shell architecture of the MSs, however, may be beneficial by helping to arrest the microcracks. Microcracks may need to take tortuous paths once they hit the MSs. On the other hand, MSs could be helpful as reinforcement in the design of resins or composites [32].

Figure 3 displays additional SEM images of ST-I MCs and size distribution histogram. Figure 3a shows the healant (SPI slurry) flowing out from a broken MC and confirms the assumption of the self-healing mechanics of the MC system. Figure 3b shows GBC nanofibers extending from a damaged MC clearly indicating the possibility of GBC combining with SPI to make a composite healant. This GBC/SPI composite would provide much higher strength than SPI alone because of the excellent tensile properties of GBC [25–27]. Figure 3c shows an image of small MCs (diameters $< 0.8 \,\mu m$) that are attached to one another, mainly because of the deposition of PLGA (most of the PVA and SPI get washed off by water).

Some MCs can also be seen covered with GBC in Fig. 3. The clustered MCs, with GBC holding them together, could make it more challenging to evenly disperse MCs in the resin. However, it is also possible that part of the GBC present on MC surfaces could migrate into the surrounding resin to enhance the MC/resin mechanical bonding. Figure 3c shows



Figure 2 SEM images of ST-I SPI-PLGA-GBC MSs produced by the spray technique.

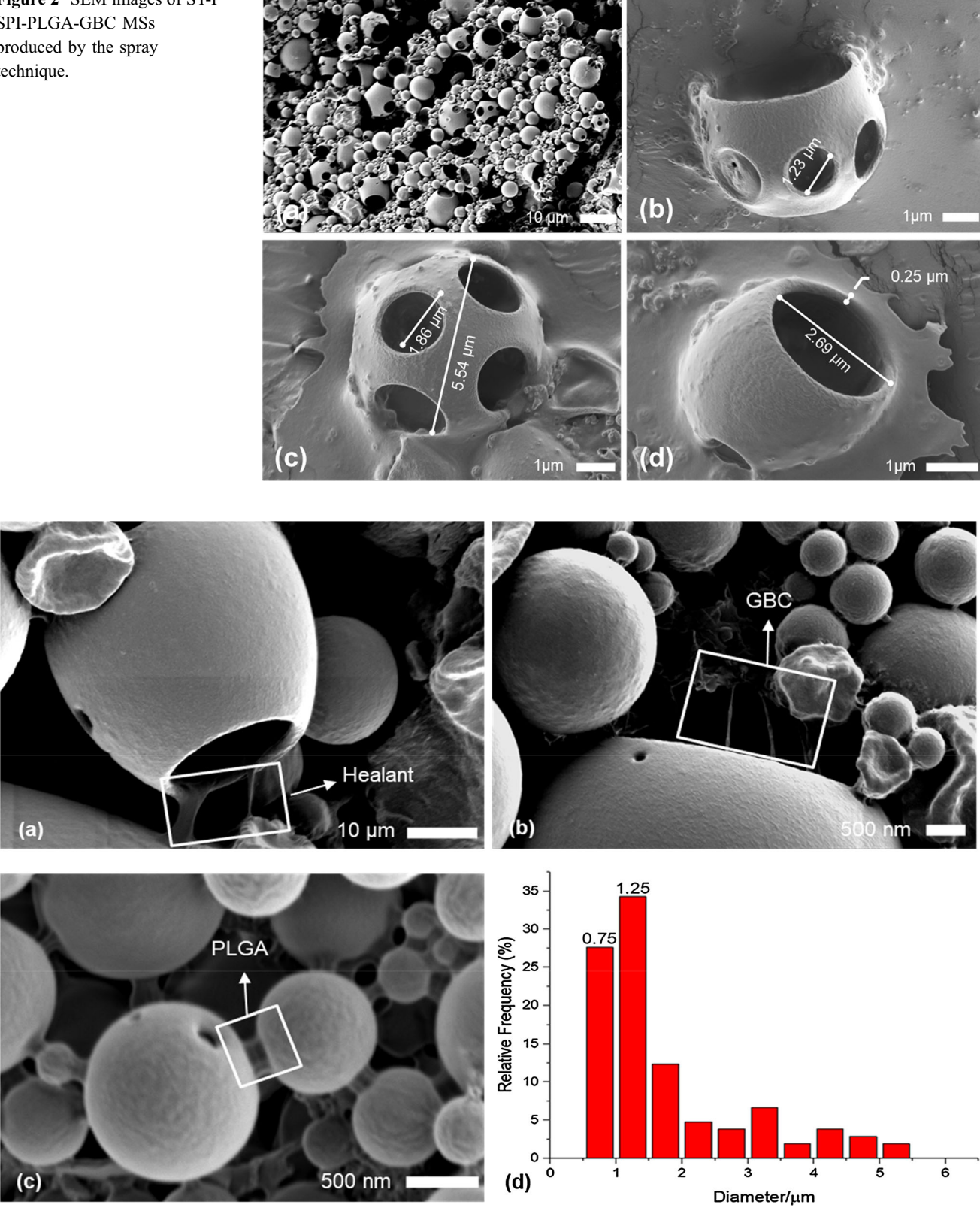


Figure 3 SEM images of ST-I SPI-PLGA-GBC MCs obtained by spray technique showing: a healing agent flowing out from a broken MC; **b** GBC protruding out from a broken MC; **c** MCs connected by GBC; **d** size distribution histogram of intact spherical MCs.



images of MCs with rough surfaces resulting from the presence of GBC. GBC migration into resin can also form a stronger and stiffer composite interphase. A strong and stiff interphase is important since it will prevent microcracks from going around the MCs rather than breaking the MCs. From the histogram of diameters of unbroken spherical MCs (N > 100) presented in Fig. 3d, the average diameter and standard deviation of the unbroken MCs are 1.75 μ m and 1.19 μ m, respectively.

MCs (ST-II) made using similar spray technique but without SDS and only half GBC amount resulted in many different shapes. This difference between the ST-I and ST-II batches may be due to the difference in stabilities of the emulsion systems. While SPI gets negatively charged after alkali treatment, SDS used in the ST-I batch is an anionic surfactant. Repulsion between SPI and SDS may disrupt the stability of ST-I emulsion causing pores in the MCs. In addition, twice as much GBC was used in ST-I batch than in ST-II batch. GBC present in the suspension may also create pores on MS surfaces by breaking the PLGA shell in ST-I. Figure 4 shows SEM images of ST-II MCs with different shapes made using this technique. The shapes include pea pod Fig. 4(a), dogbone-shaped (b), elongated (c), (d), peanut shell-like (e) and elliptical shapes (f). While it is not clear, one possible way of forming these different shapes is by coalescing of several spherical MCs that form initially. It is also possible that the elongated MCs were originally spherical but transformed into elongated MCs due to the shear forces resulting from stirring. SEM images shown in Fig. 4 possibly show different stages of the shape transformation from spherical to elliptical shapes to peanut shell-like shapes to dog bone shapes and finally the elongated ones. The highest aspect ratio of elongated MCs was 50 which is very desirable. Elongated MCs can significantly increase the probability of being in the path of the propagating microcracks and getting fractured, which, in turn, would increase the self-healing efficiency [33].

Figure 5a-c shows typical SEM images of spherical MCs (ST-II) taken at different magnifications. ST-II MCs, with average diameter of 7.59 μ m (N > 200), were significantly larger than those with average diameter of 778 nm, reported earlier by Kim and Netravali [22]. These MCs were also considerably larger than the intact ST-I MCs that had an average diameter of 1.75 µm. ST-II MCs, however, exhibited a narrower diameter distribution, with values ranging between 2.17 µm and 15.16 µm and standard deviation of 3.05 µm, as can be seen in the histogram of diameters presented in Fig. 5d. Figure 5a, b also shows spherical MCs that are coated with GBC greatly enhancing their surface roughness. Higher roughness is very desirable to increase the MC/resin interfacial adhesion through mechanical bonding. As mentioned earlier, part of the GBC nanofibers on MC surfaces can also merge into the resin during

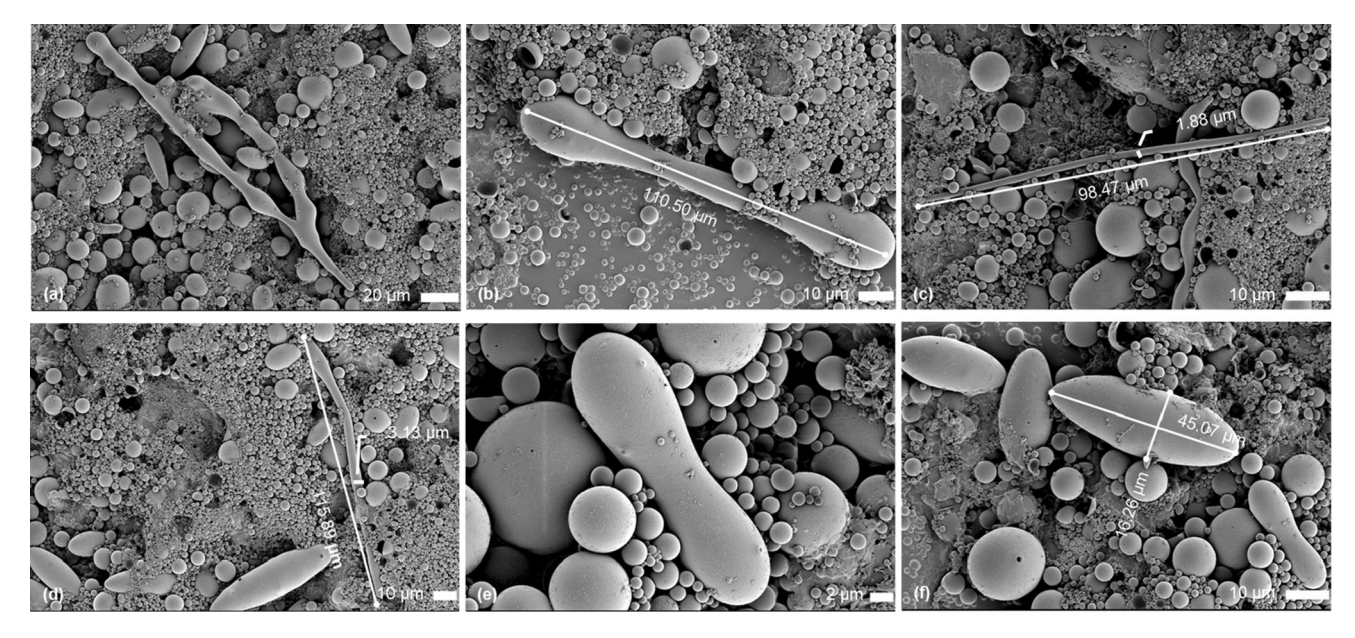


Figure 4 SEM images of ST-II SPI-PLGA-GBC MCs with different shapes created via the spray technique.



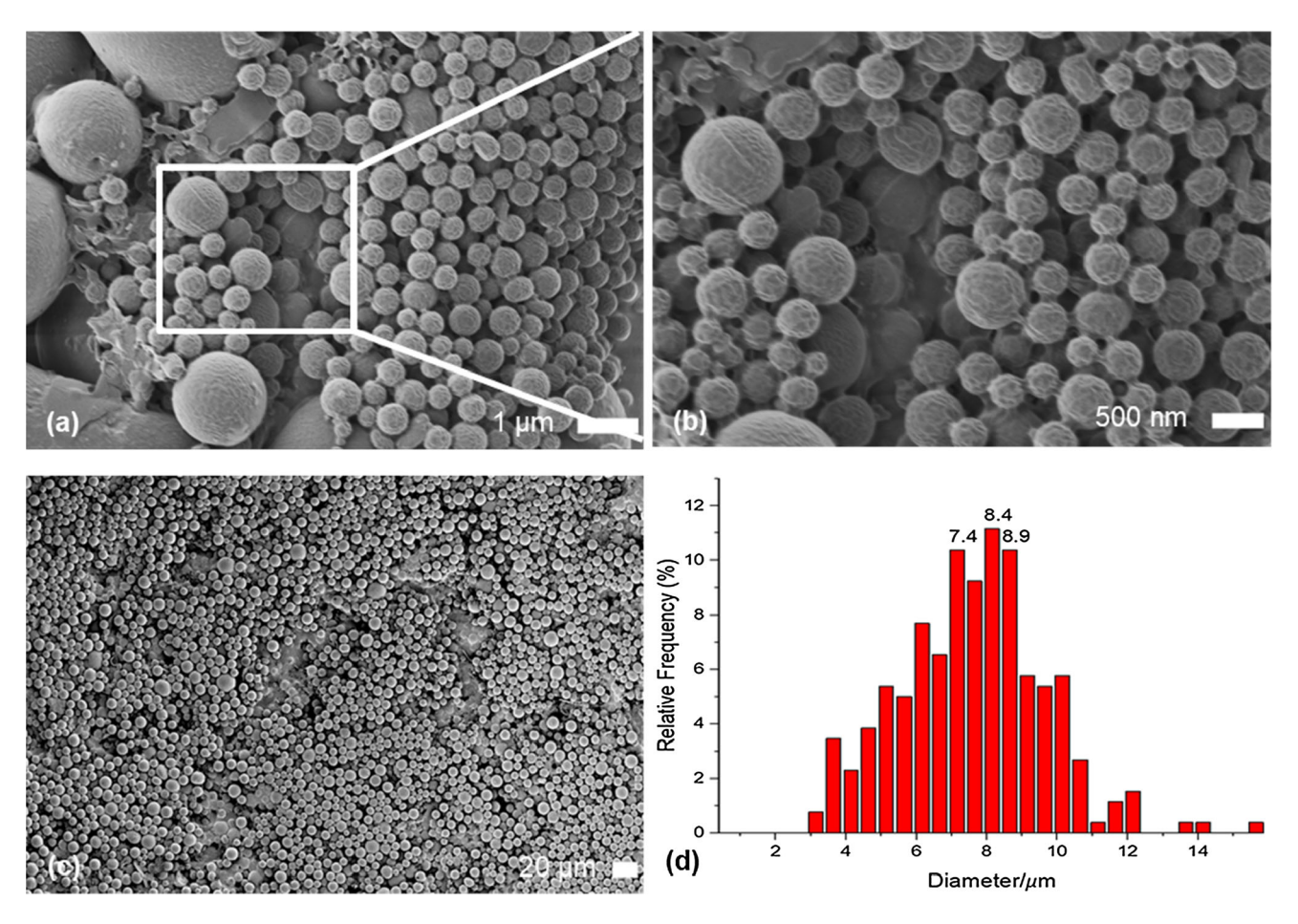


Figure 5 SEM images of spherical MCs (ST-II) prepared using spray technique: images (a) to (c) of spherical MCs at different magnifications. (d) Size distribution histogram of intact spherical MCs.

processing, making the MC/resin interphase stronger and stiffer.

Confocal laser scanning microscopy (CLSM)

Figure 6 shows fluorescent and transmission CLSM images of ST-I holey MSs that were also coated with dyed PVA and spherical MCs that are loaded with protein. The fluorescent CLSM image in Fig. 6a shows both normal MCs (without pores) and holey MSs that have black dots in them. The holey structure of the MSs can be seen as irregular contours in both fluorescent images, with weaker fluorescent signals, and those taken in transmission mode. A more intensive or brighter fluorescent (yellow) signal indicates the existence of a larger amount of SPI or PVA inside spherical MCs. Holey MSs cannot retain any healant and can be easily recognized in these images. The transmission mode image in Fig. 6b confirms these observations.

Typical CLSM images of elongated SPI-PLGA-GBC (ST-II) MCs in both fluorescent (a) and transmission (b) modes are shown in Fig. 7. As before, these images confirm the presence of healant inside ST-II MCs. The fluorescent (yellow) signal for the protein are observed in Fig. 7a, whereas the core–shell structures of both spherical and elongated MCs are shown in Fig. 7b. Elongated MCs contain more healant and can be very useful in enhancing self-healing efficiency. As stated earlier, their higher aspect ratio also increases the probability of them being in the path of the microcracks and has been shown to increase the self-healing efficiency [33].

Protein loading analysis

Protein loading is defined as the ratio of the weight of protein, in percent, within the MCs (or MSs) to the whole mass of the MCs. The ST-II specimens showed high protein loading of 10.02 wt% while ST-I



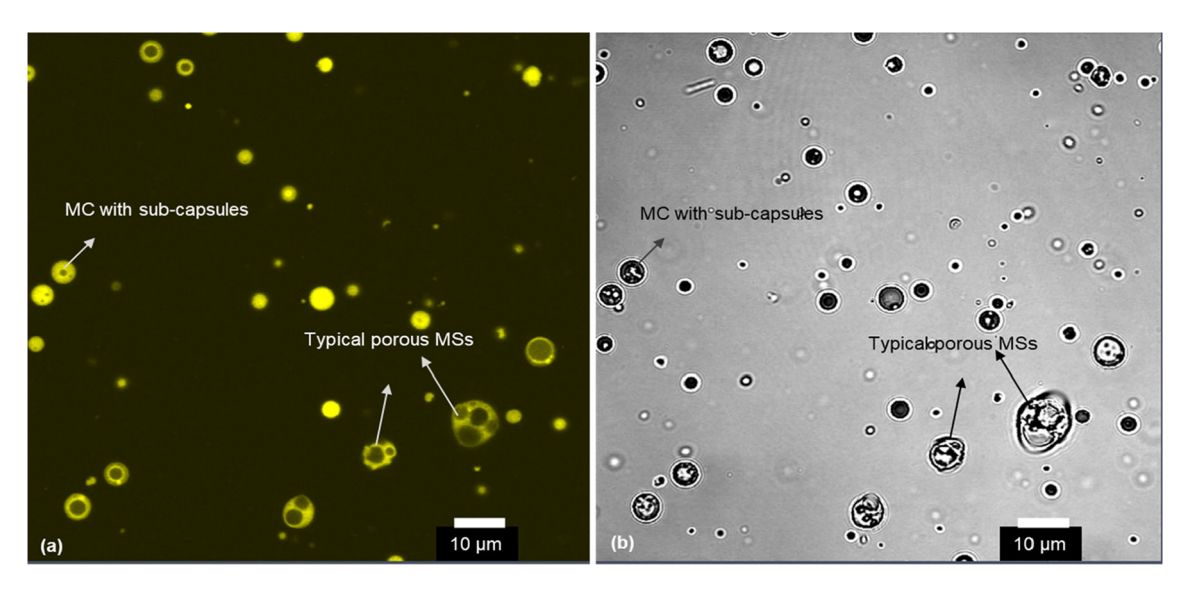


Figure 6 CLSM images showing morphologies of ST-I holey MCs and MSs (a) fluorescent image and (b) transmission image. Yellow color in the fluorescent image indicates protein (mostly) or PVA content.

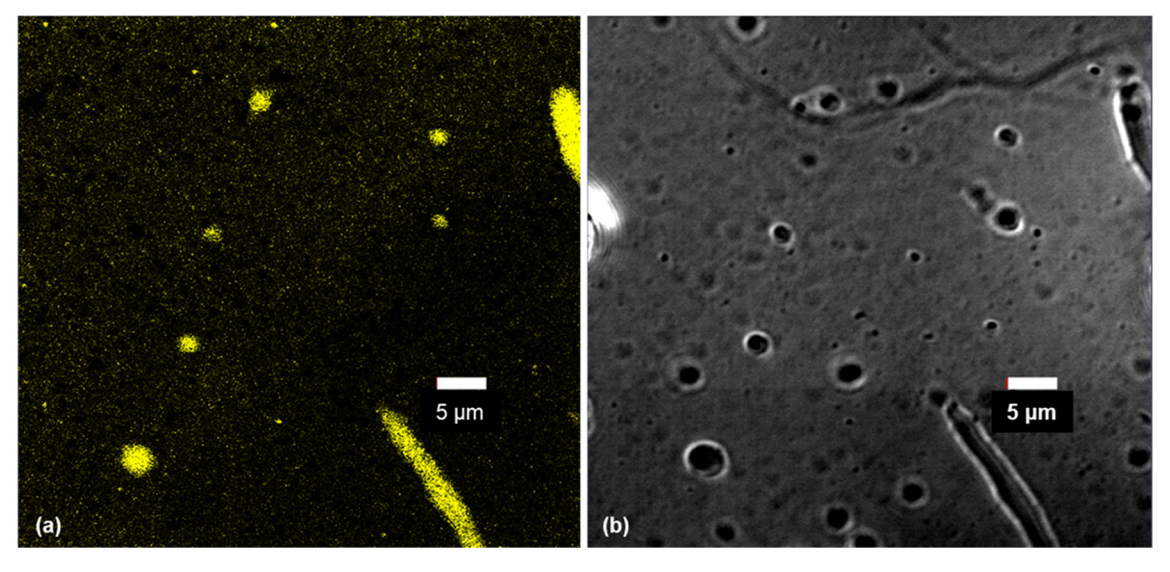


Figure 7 CLSM images of elongated ST-II MCs: a fluorescent image and b transmission image of MCs. Yellow color indicates protein (mostly) or PVA content.

specimens showed the low protein loading of just 2.25 wt%. This result is consistent with the SEM images which showed many holey MSs present in ST-I that cannot retain any SPI. In general, it is understood that the protein loading in ST-I and ST-II MCs can never be higher than the initial concentration of the protein solution of 13.67 wt% used in this study.

Attenuated total reflection-Fourier transform infrared (ATR-FTIR) analysis

Figure 8 presents ATR-FTIR spectra of pure PLGA, PVA, SPI as well as ST-I, and ST-II MCs/MSs. The PLGA spectrum shows a strong carbonyl (C = O) peak at around 1725 cm⁻¹ which is also seen in both ST-I and ST-II specimens [34]. This clearly indicates the presence of PLGA in the shells of both ST-I and ST-II MCs, as can be expected. In addition, both ST-I and ST-II specimens show bending vibration for the amine group (NH₂) from 1550 to 1650 cm⁻¹ [35]. The



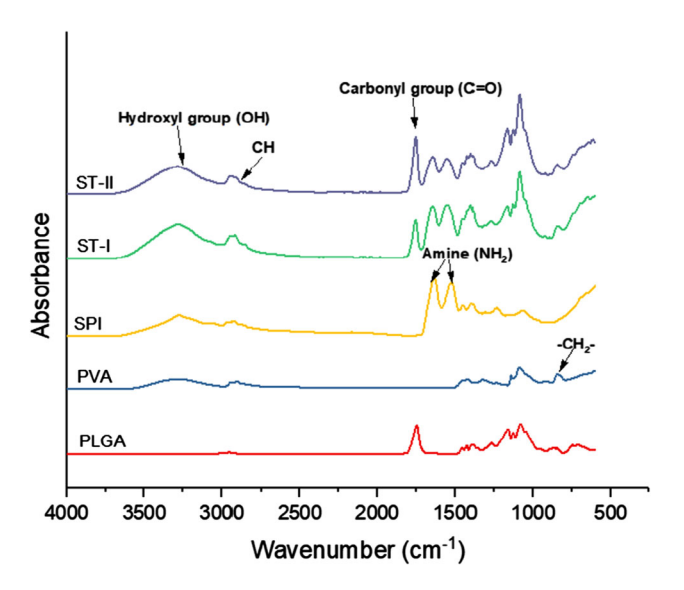


Figure 8 ATR-FTIR spectra of pure PLGA, PVA, SPI and ST-I and ST-II MCs/MSs.

valence C-H vibration at around 2900 cm⁻¹ appears in the spectra of both PVA and SPI as well as ST-I and ST-II spectra [36]. Furthermore, aliphatic -CH₂- in PVA between 750 and 850 cm⁻¹ can also be seen in the spectra of all MCs [37]. From ATR-FTIR spectra, it can be concluded that both SPI and PVA exist on the surfaces of ST-I and ST-II MCs and MSs.

Characterization of ground bacterial cellulose (GBC)

Figure 9 presents typical SEM images that show the impact of different processing steps on BC morphologies. Figure 9a shows the initial structure of freeze-dried BC pellicles in which all BC fibers are heavily stacked up in many layers and entangled with each other. Since they are continuous, no nanofiber ends can be observed. After 20 min of high-

speed wet grinding in a Ninja Ultimate Blender, the BC nanofiber network can be seen somewhat loosened up as seen in the SEM image in Fig. 9b. However, no ends are visible in the SEM image. SEM image shown in Fig. 9c is of BC after 20 min of grinding and 60 min of ball milling. It is clear that the BC nanofiber network has been disrupted and broken to a great extent (GBC). However, even after breaking, it is still difficult to spot single, separate BC nanofibers in the GBC specimen. Nevertheless, the GBC specimen does show many ends of the BC nanofibers, although they still seem to exist in a network form.

Characterization of self-healing green resins

SEM images of resin fracture surfaces

To demonstrate the self-healing behavior clearly, resins loaded with 30 wt% of ST-I or ST-II MSs/MCs and MCs were chosen. All specimens used for SEM analysis were collected after the completion of self-healing tests.

Figure 10 shows typical fracture surfaces of virgin resins without MCs/MSs. The fracture surfaces with some striations are indicative of the brittle nature of the resins such as epoxies [38]. No obvious bubbles can be observed in these images.

Figure 11 shows typical SEM images of fractures and microcracks in resin specimens loaded with 30 wt% ST-I MCs/MSs. SEM images in Fig. 11a–d show typical fracture surfaces being held together by SPI healant and GBC nanofibers. SEM images in Fig. 11b–c show fracture surfaces being connected or held together by the formation of GBC and SPI bridges, indicating the self-healing capability. SEM images in Fig. 11b, c, also show some GBC bridges with larger diameters which suggests that the BC nanofibers are

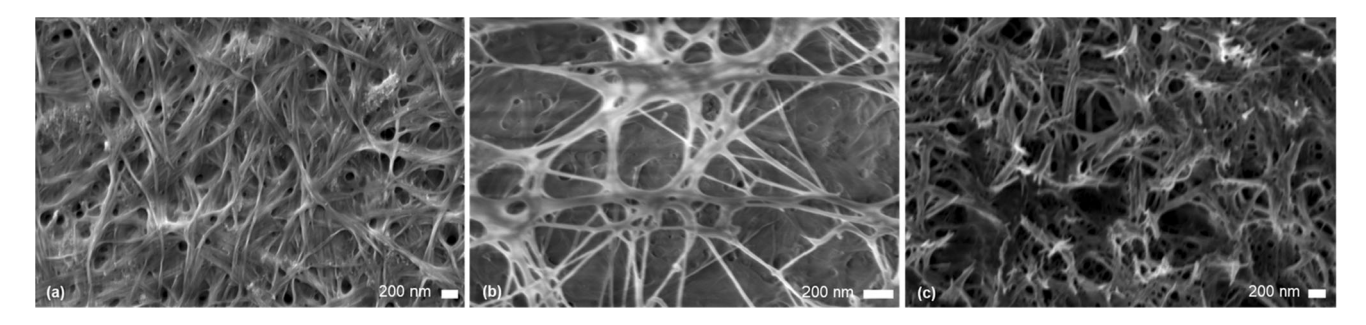
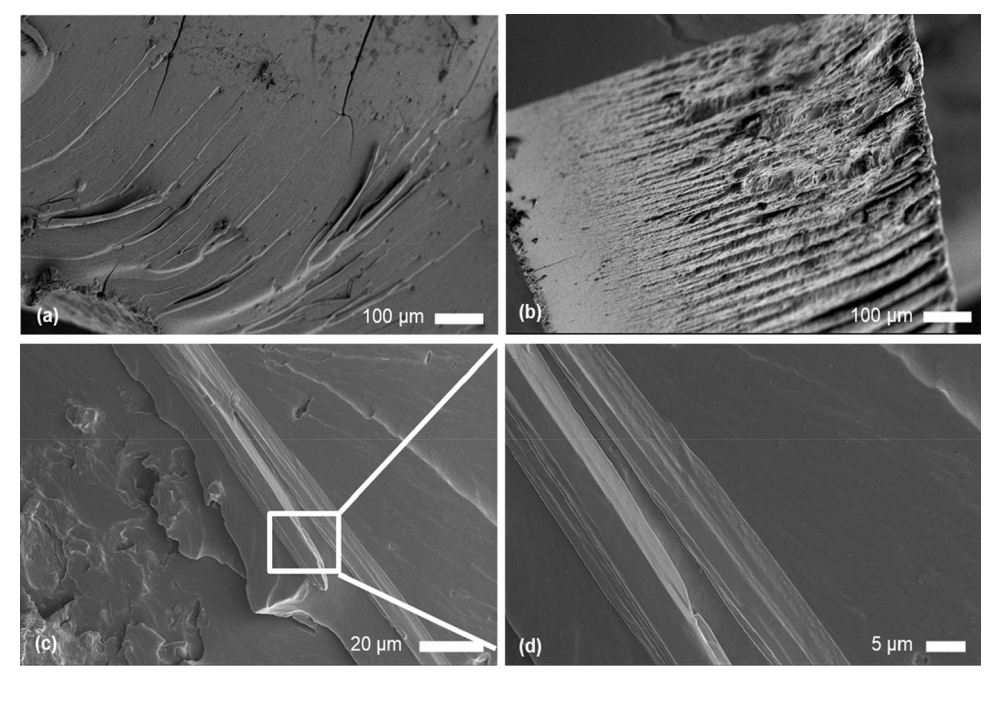


Figure 9 Typical SEM images of BC: a BC pellicle after freeze-drying; b dried BC after 20 min of grinding; c dried GBC after 20 min of grinding and 60 min of ball milling.



Figure 10 Typical SEM images of the fracture surfaces of virgin SPI resins.



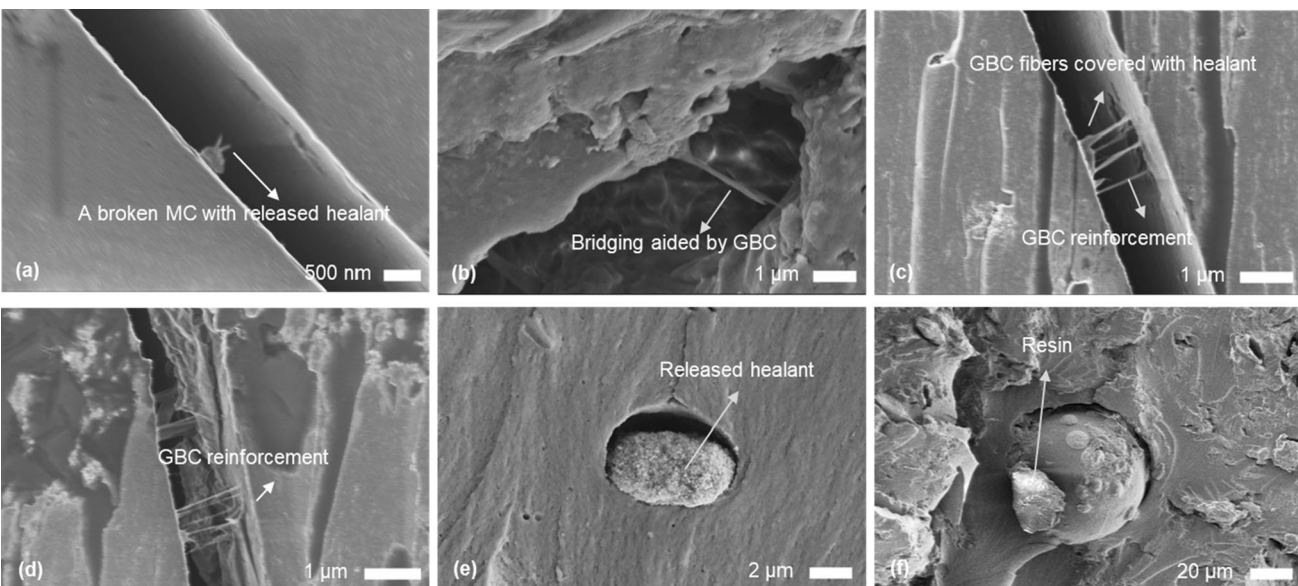


Figure 11 Typical SEM images of the fracture surfaces of SPI resins loaded with 30 wt% of ST-I MCs/MSs showing incorporation of GBC into the resin.

bunched up. Most of them are also covered with SPI resin forming composite bridges. It is intuitive that GBC/SPI composite healant will have higher bond strength than pure SPI because of the high strength of BC. In fact, the primary goal of this research was to use SPI containing GBC as the composite healant. The advantage of SPI slurry with GBC as the healant is that fluid is easier to stay attached to the convex surface via the Coandă effect discussed earlier by

Katopodes [39]. In the present case, the SPI slurry is seen to flow along the GBC fibers. These results confirm that the presence of GBC is beneficial for forming bridging zones. In the absence of GBC, the SPI slurry, on its own may be less likely to form bridges because of the surface tension. SEM image in Fig. 12e shows healant leaching out of a broken MC. An unbroken MC seen in Fig. 11f seems to have a coating of SPI resin. This cohesive failure of SPI resin



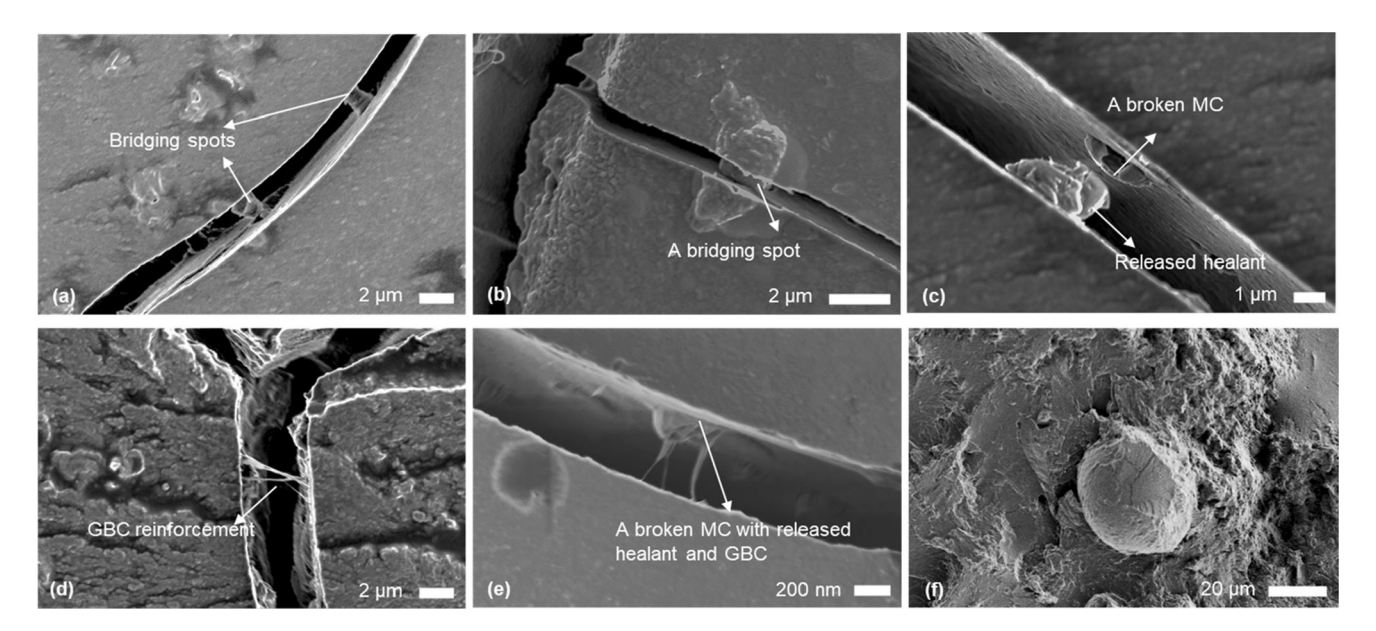


Figure 12 Typical SEM images of microcracks and fracture surfaces of SPI resins loaded with 30 wt% of ST-II MCs.

implies that the interfacial bonding between MCs and resins was at least as strong as the resin itself.

Figure 12 shows typical SEM images of microcracks and fracture surfaces of SPI resins loaded with 30 wt% of ST-II MCs. It can be seen in SEM images in Figs. 12a, b that the healing agent released from broken ST-II MCs is able to form many bridges within the microcracks, as in the earlier case. It is also clear, as with ST-I MCs, that the bridges formed are far apart. This suggests that more healant, i.e., more MCs, would be needed to form more bridges to improve the self-healing efficiency further. However, as discussed later and found by other researchers, increasing MC loading beyond the optimum level results in an undesirable lowering of the mechanical properties of the resin [28].

SEM image in Fig. 12c shows the shell of a MC that looks debonded from the resin with no healing agent coming out from it. This demonstrates an undesirable situation where the microcrack passes around the MC without fracturing it, and hence, no bridging or self-healing can occur. This also indicates a clear need for further improving the MC/resin bonding to enhance the self-healing efficiency.

It can be observed from the SEM images in Fig. 12d, e that GBC fibers extend in between the fracture surfaces with SPI resin attached to their surfaces, forming similar composite bridges. SEM image in Fig. 12f shows a MC on the fracture surface. Some SPI resin sticking to the MC surface indicates

that the MC/resin interfacial adhesion is good. This is believed to be due to the GBC present on the MC surfaces getting incorporated into the resin surrounding the MC.

Mechanical properties of the resin

Resins were characterized for their tensile properties as a function of ST-I MC/MS and ST-II MC loading. Statistical analysis was performed on the resin failure load in self-healing tests via the two-tailed unequal variance t-test with 95% confidence interval. Figure 13 shows the effect of ST-I MC/MS and ST-II MC loading on the resin failure load (indicator of strength) during the self-healing efficiency tests. Resin failure load data, in the form of histograms, are shown in Fig. 13a, and load vs elongation plots obtained during self-healing tests for different resins are shown in Fig. 13b, c. Results for both ST-I and ST-II loaded resins showed that there is an optimum MC/MS loading (wt%) beyond which there is an undesirable drop in strength. The addition of both ST-I or ST-II MCs/MSs improved the strength of the resin up to 20 wt% MC/MS loading as compared to control resins without MCs. At higher MC/MS loading of 30 wt%, however, both resins showed significant decreases in strength. In spite of the drop in strength of resins with 30 wt% MC/MS loading, the strength was still higher than that of the control resin. Many earlier studies had suggested that adding



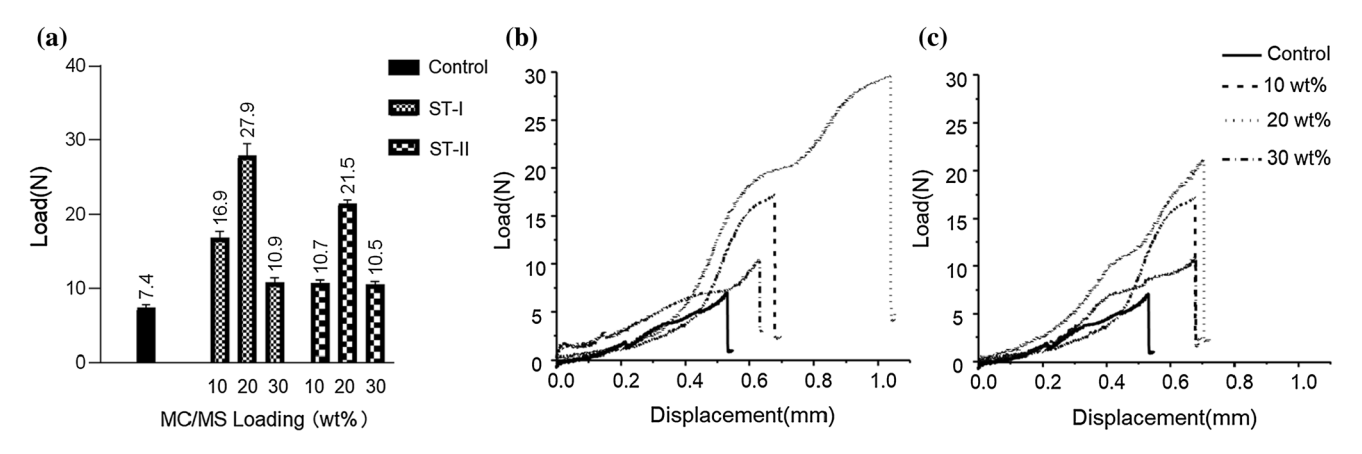


Figure 13 a Effect of MC/MS loading on resin failure load in self-healing efficiency tests; **b** and **c** load vs displacement plots in self-healing test with different MC/MS loadings: **b** resins with ST-I MCs/MSs and **c** resins with ST-II MCs.

MCs invariably decreases the resin strength [33]. The improvement in strength seen here may be attributed to the presence of GBC on the surface of the MCs that gets incorporated, at least partially, into the resin to form a composite layer in and around the MCs forming a stronger interphase region. Thus, adding GBC not only can increase the MC/resin bonding but also strengthen the resin. Higher strength may also be due to the existence of some elongated MCs, although this is not very clear.

Resins with ST-I MCs/MSs showed significant enhancement in strength compared to resins with ST-II MCs at all loading levels, more so at 10 and 20 wt%. This implies that the ST-I MCs, which also contain holey MSs, may be beneficial for mechanical improvement.

Figure 14 depicts the effect of ST-I and ST-II MC/MS loadings on the toughness (area under the curve) of the resins in self-healing efficiency tests. Resins loaded with both ST-I and ST-II MCs and MSs greatly

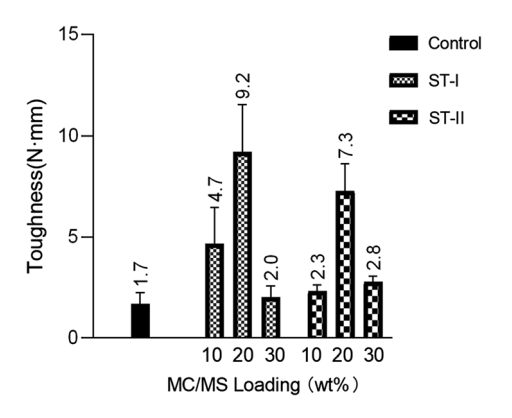


Figure 14 Effect of MC/MS loading on the resin toughness in self-healing efficiency tests.

improved their toughness at 10 and 20 wt% loadings compared to control resin. The sharp drop in the toughness of resins containing ST-I MCs/MSs and ST-II MCs at 30 wt% loading was due to their lower fracture strains. Similarly, it can be observed that ST-I MCs/MSs enhanced the resin toughness better than ST-II. One possible explanation for this is that the holey MSs in ST-I are able to arrest the microcracks and absorb energy. Holey MSs do have larger contact (interface) areas (outer and inner surfaces) than solid MCs, and as a result, debonding them from the resin would consume higher amount of energy than intact MCs.

Figure 15 depicts the effect of MC/MS loading on tensile stress vs strain characteristics and resin modulus values obtained from these tests. It can be observed that the moduli of all SPI resins containing ST-I and ST-II MCs/MSs increased significantly compared to the control resin. However, resins with 20 wt% loading of both ST-I and ST-II MCs/MSs showed the highest values. As stated earlier, it is possible that this improvement is probably due to the GBC layer surrounding the MC shell that gets incorporated into the resin, at least partly, forming a strong interphase layer as well as improving the MC/ resin interfacial bonding. Moduli of resins containing both ST-I and ST-II MCs/MSs, however, decreased sharply when MCs/MSs loadings increased to 30 wt%. This result suggests that at higher loading MCs start to act as defects, possibly, due to aggregation [33].



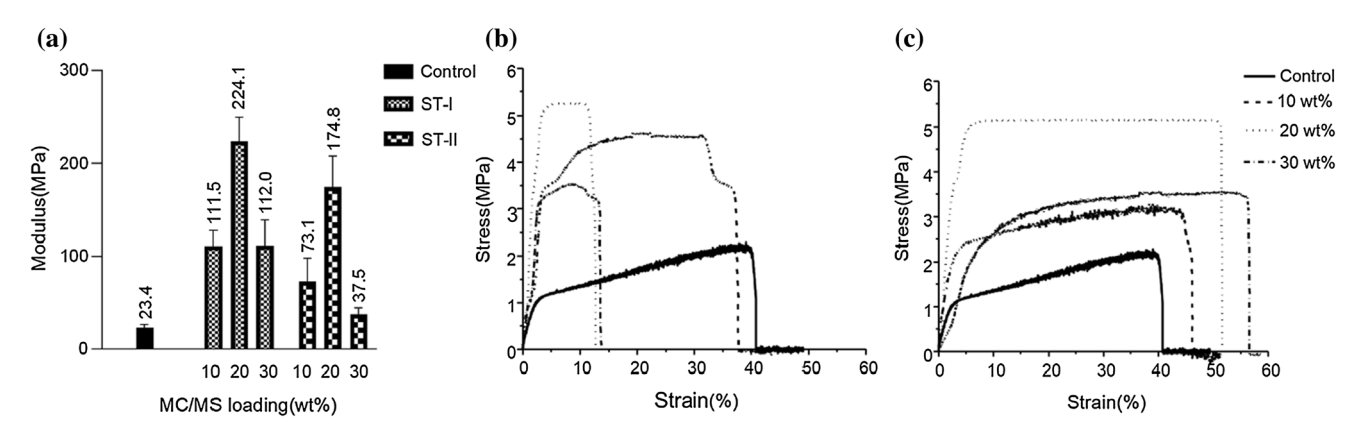


Figure 15 a Effect of MC/MS loading on the resin modulus values obtained from the tensile tests; **b** and **c** typical stress vs strain plots in tensile test at different MC/MS loading levels: **b** resins with ST-I MCs/MSs and **c** resins with ST-II MCs.

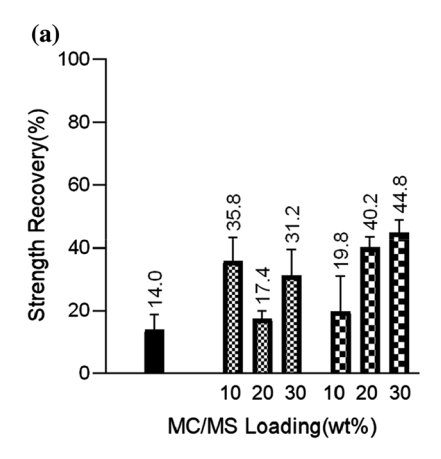
Self-healing efficiency

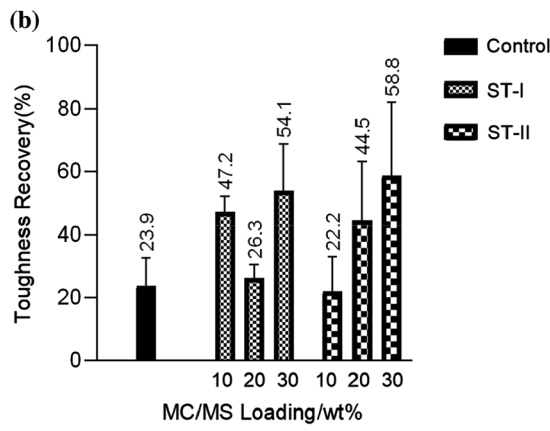
Figure 16 presents self-healing efficiencies of SPI resins as a function of ST-I and ST-II MC/MS loading. It is clear that resins containing ST-II MCs showed significantly higher self-healing efficiencies of up to about 45% for strength recovery and 59% for toughness recovery. Also, as expected, SPI resins with higher MC loadings showed higher self-healing efficiencies for resins that contained ST-II MCs but not for resins with ST-I MCs/MSs. This could be attributed to the combined effect of enhanced mechanical properties and decreased self-healing ability of resins containing ST-I MCs/MSs. As discussed earlier, ST-I MCs/MSs exhibited high potential to improve resin strength as well as toughness. Having MSs enhanced the mechanical properties of the resin but the lack of healant availability (only 2.25% protein loading) reduced the ability to 'self-heal'. On the other hand, resins with ST-II MCs showed higher strength recovery of 45% at 30 wt% MCs loading. This is

clearly because of higher protein loading of 10 wt% which provides much higher amount of healant within the microcracks for better self-healing. In addition, the elongated morphology of ST-II MCs is also helpful in increasing the probability of the MCs being in the path of the propagating microcracks [33]. Resins with ST-II MCs resulted in higher toughness recovery as well. For example, at 30 wt% ST-II MC loading the self-healing efficiency in toughness was 59%. In addition to higher availability of the healant this was also due to better ability to bridging fracture surfaces provided by the GBC.

Earlier study of soy protein resins and SPI healant, by Kim and Netravali showed self-healing efficiencies of up to 48% [22]. Another study of zein proteins reported self-healing efficiency of fracture stress as high as 72% [33]. A study of starch-based resin reported self-healing efficiency of 66% [28]. While the results in this study are comparable to the earlier study on soy resin for self-healing efficiency in terms of strength, the self-healing efficiency in terms of

Figure 16 Self-healing efficiencies of SPI resins as a function of MC/MS loadings: a strength recovery (resin failure load); b toughness recovery.







toughness is much better. The results also suggest that there is scope to improve the self-healing efficiency further. This may be achieved by increasing the healant (protein + GBC) loading in the MCs, increasing aspect ratios of MCs and/or by obtaining better covering of MCs by GBC.

Conclusions

The main goal of this research was to prepare MCs with higher aspect ratios containing GBC/SPI composite healant. Effects of morphology, shape/size and protein loading of MCs, incorporation of GBC in MCs as well as MC loading in the resin on self-healing efficiencies of soy protein-based resin were studied. The main conclusions are stated below.

- Spray technique was found to be useful in producing combination of elongated, elliptical, dog bone, rodlike and spherical MCs. Aspect ratios of the elongated capsules were as high as 50.
- ST-I specimens that contained both MCs and holey MSs resulted in enhanced mechanical properties of the resin while the healing efficiency was low as a result of low protein loading.
- ST-II specimens contained MCs that had spherical as well as various other shapes. While all MCs successfully encapsulated both SPI and GBC, many of them were also covered with GBC.
- GBC-covered MCs showed better MC/resin adhesion because of the increased surface roughness of the MCs and also because part of the GBC got incorporated with the surrounding resin forming a strong interphase region. Combining GBC with SPI created a composite healant that formed stronger bridges between fracture surfaces and resulted in higher self-healing efficiency.
- Self-healing efficiencies of about 45% for fracture strength and 59% for toughness were obtained. This suggests that there is good scope to improve self-healing efficiencies further by increasing both protein and GBC loading in the MCs as well as by increasing aspect ratios of MCs.
- For resins loaded with ST-II MCs, increased MC loading from 10 to 30 wt% resulted in enhanced self-healing efficiencies. However, 20 wt% MC loading was found to be optimal and at 30 wt%

MC loading the tensile properties of the resin decreased.

Acknowledgements

This work made use of the Cornell Center for Materials Research shared facilities which are supported through the NSF MRSEC program (DMR-1719875).

Funding

This study was not funded by any grant.

Declarations

Conflict of interest The authors declare that they have no conflict of interest.

Supplementary Information: The online version contains supplementary material available at https://doi.org/10.1007/s10853-021-06066-y.

References

- [1] Hannah R (2017) Fossil fuels. In: Our World data. our-worldindata.org/fossil-fuels. Accessed 9 Jul 2020
- [2] Geyer R, Jambeck JR, Law KL (2017) Production, use, and fate of all plastics ever made. Sci Adv 3:e1700782. https://d oi.org/10.1126/sciadv.1700782
- [3] Maniiyan VP (2017) Soy protein: introduction, structure and properties relationship. Soy protein-based blends. Composites and Nanocomposites. John Wiley & Sons Inc, Hoboken, NJ, pp 23–37
- [4] Vnučec D, Kutnar A, Goršek A (2017) Soy-based adhesives for wood-bonding. J Adhes Sci Technol 31:910–931. http s://doi.org/10.1080/01694243.2016.1237278
- [5] Wolf WJ (1970) Soybean proteins: their functional, chemical, and physical properties. J Agric Food Chem 18:969–976. https://doi.org/10.1021/jf60172a025
- [6] Souzandeh H, Johnson KS, Wang Y, Bhamidipaty K, Zhong WH (2016) Soy-protein-based nanofabrics for highly efficient and multifunctional air filtration. ACS Appl Mater Interf 8:20023–20031. https://doi.org/10.1021/acsami.6b 05339
- [7] Wang Y, Mo X, Sun XS, Wang D (2007) Soy protein adhesion enhanced by glutaraldehyde crosslink. J Appl Polym Sci 104:130–136. https://doi.org/10.1002/app.24675



- [8] Kim SY, Sottos NR, White SR (2019) Self-healing of fatigue damage in cross-ply glass/epoxy laminates. Compos Sci Technol 175:122–127. https://doi.org/10.1016/j.compscitec h.2019.03.016
- [9] Kim JR, Netravali AN (2017) Self-healing green composites based on soy protein and microfibrillated cellulose. Compos Sci Technol 143:22–30. https://doi.org/10.1016/j.compscite ch.2017.02.030
- [10] Norris CJ, Meadway GJ, O'Sullivan MJ, Bond IP, Trask RS (2011) Self-healing fibre reinforced composites via a bioinspired vasculature. Adv Funct Mater 21:3624–3633. https://d oi.org/10.1002/adfm.201101100
- [11] Kang J, Son D, Wang GJN, Liu Y, Lopez J, Kim Y, Oh JY, Katsumata T, Mun J, Lee Y, Jin L, Tok JBH, Bao Z (2018) Tough and water-insensitive self-healing elastomer for Robust electronic skin. Adv Mater 30:13. https://doi.org/10. 1002/adma.201706846
- [12] Thakur VK, Kessler MR (2015) Self-healing polymer nanocomposite materials: a review. Polymer (Guildf) 69:369–383
- [13] Lee MW, An S, Lee C, Liou M, Yasin AL, Yoon SS (2014) Hybrid self-healing matrix using core-shell nanofibers and capsuleless microdroplets. ACS Appl Mater Interf 6:10461–10468. https://doi.org/10.1021/am5020293
- [14] Van Der Zwaag S, Grande AM, Post W, Garcia SJ, Bor TC (2014) Review of current strategies to induce self-healing behaviour in fibre reinforced polymer based composites. Mater Sci Technol (UK) 30:1633–1641. https://doi.org/10. 1179/1743284714Y.0000000624
- [15] Mauldin TC, Kessler MR (2010) Self-healing polymers and composites. Int Mater Rev 55:317–346. https://doi.org/10. 1179/095066010X12646898728408
- [16] Mostavi E, Asadi S, Hassan MM, Alansari M (2015) Evaluation of self-healing mechanisms in concrete with double-walled sodium silicate microcapsules. J Mater Civ Eng 27:04015035. https://doi.org/10.1061/(ASCE)MT.1943-553 3.0001314
- [17] Ferguson JB, Schultz BF, Rohatgi PK (2014) Self-healing metals and metal matrix composites. JOM 66:866–871
- [18] Guo M, Li W, Han N, Wang J, Su J, Li J, Zhang X (2018) Novel dual-component microencapsulated hydrophobic amine and microencapsulated isocyanate used for self-healing anti-corrosion coating. Polymers (Basel) 10:319–334. h ttps://doi.org/10.3390/polym10030319
- [19] O'Donnell PB, McGinity JW (1997) Preparation of microspheres by the solvent evaporation technique. Adv Drug Deliv Rev 28:25–42
- [20] Xue Y, Ye YS, Chen FY, Wang H, Chen C, Xue ZG, Zhou XP, Xie XL, Mai YW (2016) A simple and controllable graphene-templated approach to synthesise 2D silica-based

- nanomaterials using water-in-oil microemulsions. Chem Commun 52:575–578. https://doi.org/10.1039/c5cc06941f
- [21] Bagale UD, Sonawane SH, Bhanvase BA, Kulkarni RD, Gogate PR (2018) Green synthesis of nanocapsules for selfhealing anticorrosion coating using ultrasound-assisted approach. Green Process Synth 7:147–159. https://doi.org/ 10.1515/gps-2016-0160
- [22] Kim JR, Netravali AN (2016) Self-healing properties of protein resin with soy protein isolate-loaded poly(_{D,L}-lactide-co-glycolide) microcapsules. Adv Funct Mater 26:4786–4796. https://doi.org/10.1002/adfm.201600465
- [23] Malo De Molina P, Zhang M, Bayles AV, Helgeson ME (2016) Oil-in-water-in-oil multinanoemulsions for templating complex nanoparticles. Nano Lett 16:7325–7332. http s://doi.org/10.1021/acs.nanolett.6b02073
- [24] Kim JR, Netravali AN (2017) Parametric study of proteinencapsulated microcapsule formation and effect on selfhealing efficiency of 'green' soy protein resin. J Mater Sci 52:3028–3047. https://doi.org/10.1007/s10853-016-0588-y
- [25] Seoane IT, Cerrutti P, Vazquez A, Manfredi LB, Cyras VP (2017) Polyhydroxybutyrate-based nanocomposites with cellulose nanocrystals and bacterial cellulose. J Polym Environ 25:586–598. https://doi.org/10.1007/s10924-016-0 838-8
- [26] de Oliveira Barud HG, da Silva RR, da Silva BH, Tercjak A, Gutierrez J, Lustri WR, de Oliveira Junior OB, Ribeiro SJL (2016) A multipurpose natural and renewable polymer in medical applications: bacterial cellulose. Carbohydr Polym 153:406–420. https://doi.org/10.1016/j.carbpol.2016.07.059
- [27] Kalashnikova I, Bizot H, Cathala B, Capron I (2011) New pickering emulsions stabilized by bacterial cellulose nanocrystals. Langmuir 27:7471–7479. https://doi.org/10.1 021/la200971f
- [28] Kim JR, Netravali AN (2017) Self-healing starch-based 'green' thermoset resin. Polymer (Guildf) 117:150–159
- [29] Netravali AN (2018) Self-healing green polymers and composites. Advanced green composites. John Wiley & Sons Inc, Hoboken, NJ, pp 135–185
- [30] ASTM E647-00 Standard test method for measurement of fatigue crack growth rates. www.astm.org/DATABASE.CA RT/HISTORICAL/E647-00.htm. Accessed 8 Jul 2020
- [31] Hora MS, Rana RK, Nunberg JH, Tice TR, Gilley RM, Hudson ME (1990) Release of human serum albumin from poly(lactide-co-glycolide) microspheres. Pharm Res 7:1190–1194. https://doi.org/10.1023/A:1015948829632
- [32] White SR, Sottos NR, Geubelle PH, Moore JS, Kessler MR, Sriram SR, Brown EN, Viswanathan S (2001) Autonomic healing of polymer composites. Nature 409:794–797
- [33] Souzandeh H, Netravali AN (2019) Self-healing of 'green' thermoset zein resins with irregular shaped waxy maize



- starch-based/poly(_{D,L}-lactic-co-glycolic acid) microcapsules. Compos Sci Technol 183:107831. https://doi.org/10.1016/j.compscitech.2019.107831
- [34] Paragkumar NT, Edith D, Six JL (2006) Surface characteristics of PLA and PLGA films. Appl Surf Sci 253:2758–2764. https://doi.org/10.1016/j.apsusc.2006.05. 047
- [35] Combs JD (2016) Surface FTIR techniques to analyze the conformation of proteins/peptides in H2O environment. J Phys Chem Biophys. https://doi.org/10.4172/2161-0398. 1000202
- [36] Belfer S, Fainchtain R, Purinson Y, Kedem O (2000) Surface characterization by FTIR-ATR spectroscopy of polyethersulfone membranes-unmodified, modified and protein fouled. J Memb Sci 172:113–124. https://doi.org/10.1016/ S0376-7388(00)00316-1

- [37] Prosanov IY, Matvienko AA (2010) Study of PVA thermal destruction by means of IR and Raman spectroscopy. Phys Solid State 52:2203–2206. https://doi.org/10.1134/ S1063783410100318
- [38] Netravali AN, Henstenburg RB, Phoenix SL, Schwartz P (1989) Interfacial shear strength studies using the singlefilament-composite test. I: Experiments on graphite fibers in epoxy. Polym Compos 10:226–241. https://doi.org/10.1002/ pc.750100405
- [39] Katopodes ND (2019) Ideal Fluid Flow. In: Free-Surface Flow. Elsevier, pp 428–515

Publisher's Note Springer Nature remains neutral with regard to jurisdictional claims in published maps and institutional affiliations.

